Plasma Behaviours and Magnetic Field Distributions of a Short-Pulse Laser-Assisted Pulsed Plasma Thruster

IEPC-2015-109／ISTS-2015-b-109

Presented at Joint Conference of 30th International Symposium on Space Technology and Science
34th International Electric Propulsion Conference and 6th Nano-satellite Symposium,
Hyogo-Kobe, Japan
July 4 – 10, 2015

Nao Akashi, Hiroto Moriya, Yuji Oigawa, Hiroshi Hosokawa, Hideyuki Horisawa
Department of Aeronautics and Astronautics, Tokai University, Hiratsuka, Kanagawa, 259-1292, Japan

To observe the plasma acceleration process and to understand the mechanism of high speed plasma generation between the rectangular electrodes of a short-pulse laser-assisted pulsed plasma thruster (LA-PPT), observation of plasma behaviors by an ICCD camera and measurement of magnetic field distributions by magnetic probes were conducted. From the time-resolved ICCD images, behaviors of the plasma wavefront were analyzed. From the results of time-resolved images, the strong emission regions were found at near electrodes and propellant surface. Furthermore, it was confirmed that no strong correlations between discharge current and plasma emissions could be extracted. In addition, temporal variations of magnetic field distributions were measured by magnetic field probes located at various positions for Vc = 8,000 V (C = 24, 50 nF). From the result, magnetic field was induced in a whole region in the discharge channel and was oscillating with similar frequency to that of discharge current for C = 24 nF. On the other hand, for the C = 50 nF, the strength of magnetic field was decreasing with increasing distance from the propellant surface. It was confirmed that magnetic field strength in near surface region of x = 0 ~ 10 mm was much stronger than those measured in the other regions.

Nomenclature

$\boldsymbol{B}$	=	magnetic field
dt	=	time step
N	=	winding number of magnetic field probe
V_c	=	capacitor voltage
I	=	ampere of discharge
Isp	=	specific impulse
h	=	electrode height
V_c	=	capacitor voltage
C	=	capacitor capacitance

I. Introduction

The current trend towards small spacecraft, which is not only mass limited but also power limited, has produced a strong interest in development of micropropulsion devices.[1-4] The significance in reducing launch masses has attracted growing interests in regard to a decrease in mission cost and an increase in launch rate. Although, in the past, many very small spacecraft lacked propulsion systems, future microspacecraft will require significant propulsion capability to provide a high degree of maneuverability and capability. The benefit of using electric propulsion for the reduction of spacecraft mass will likely be even more significant for mass limited micro-spacecraft missions.[2-4] Feasibility studies of micro-spacecraft are currently under development for a mass less than 100 kg with an available power level for propulsion of less than 100 watts. [2-4] Various potential propulsion systems for micro- spacecraft applications, such as ion thrusters, field emission thrusters, pulsed plasma thrusters (PPTs), vaporizing liquid thrusters, resistjets, microwave arcjets, pulsed arcjets, etc., have been proposed and are under significant development for primary and attitude control applications. [4] In particular, the PPTs are expected to be used for microsatellites and their longterm missions because of the precise impulse bit controllability.

On the other hand, small-sized onboard laser plasma thrusters are also under significant development with rapid evolutions of novel compact laser systems. One of the advantages of the laser thrusters is that they can induce high specific impulses. In addition, the system can be very simple and small with significant controllability of the thrust. [5-8] To improve thrust performances and system simplicities of those conventional electric and laser propulsion systems, a preliminary study on a laser-electric hybrid acceleration system have been conducted by the authors.[9-15]

II. Laser assisted pulsed plasma thruster

A schematic of the rectangular laser-assisted pulsed plasma thruster (LA-PPT) is illustrated in Fig. 1.[9-15] A basic idea of the system is that a bunch of laser-ablation plasma, induced through laser irradiation on a solid target, is supplied to an acceleration channel and additionally accelerated by electrical means between an anode and a cathode. When the current between the electrodes increases, the plasma can be heated and further ionized through joule heating. Thus, the electrothermal acceleration effect will be significant. With larger current exceeding more than one thousand amperes, the electromagnetic acceleration effect becomes significant. With the interaction of the current and a self-induced magnetic field, a streamwise acceleration of the plasma will be provided.[17, 18]

Since any solid materials can be used for the propellant in these systems, no tanks, no valves, or piping systems are required for the propulsion system. Also, various materials in any phases can be used for the propellant. Therefore, the system employing this technique can be simple and compact. As the laser-ablation plasma has a directed initial velocity of tens of km/s, which will be further accelerated by electrical means, significantly high specific impulses can be expected.

III. . Research motivation

Figure 2 shows the typical high specific impulse characteristics of the laser-assisted pulsed plasma thruster replotted from our previous report, in which variations of specific impulse with charge energy are plotted for various acceleration channel configurations[15]. From the figure, it can be seen in all the cases that specific impulse increased with the increase of the charge energy. Moreover, thrusters with longer channel length showed higher specific impulses. The highest specific impulse of 7,200 sec was obtained with the 10 mm x 50 mm thruster at the highest charge energy of 8.6 J. However, the mechanism of generation of high specific impulses, or namely high speed plasmas, is still unknown.

Therefore, an objective of this study is to observe the plasma acceleration process from the results of image data. To observe the plasma behaviors between the rectangular electrodes of the LA-PPT in short pulse operation and high voltage operation, an ICCD camera was utilized.

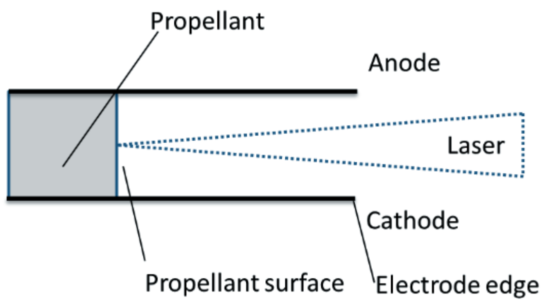

Figure1. Schematic of illustration of a rectangular laser-assisted pulsed plasma thruster (LA-PPT).

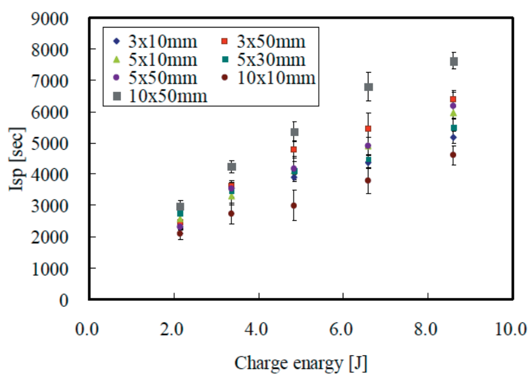

Figure2. Variation of specific impulse with charging energy for thrusters with various electrode geometries (electrode length × electrode height).[15]

IV. Experimental set up of Plasma behavior analysis

A. Plasma plume observation with ICCD camera

To observe the plasma behaviors between the rectangular electrodes of the LA-PPT, the time-resolved imaging with an ICCD camera was conducted. From the time-resolved images, behaviors of the plasma wave front were analyzed and speeds of the plasmas were estimated.

A photo of the thruster is shown in Fig. 3, in which electrodes made of copper and propellant and insulator made of alumina ceramics. A capacitor bank (TDK, Ultra-high Voltage Ceramic Capacitors UHV-3A, capacitance: 4 ,6nF, total capacitance of capacitor bank: 24 , 50nF) Configuration of the thruster is listed in Table 1. In this study, based on our previous results [16)], relatively larger width and length of the rectangular electrodes of 10 mm x 50 mm were utilized, which showed the best thrust performance among various electrode configurations in our previous study.

A schematic of experimental set up for ICCD camera observation is shown in Fig. 4. The LA-PPT is placed in vacuum chamber (2.7×10^{-3} Pa) and ignited through a laser ablation plasma induced with a focused laser pulse at a center surface of the propellant. As for the laser oscillator, an Nd:YAG laser (CONTINUUM INC., Surelite II, wavelength: 1,064 nm, pulse width 5 ns, pulse energy: 400 mJ) was utilized. Time-resolved images were monitored with an ICCD camera (ANDOR TECHNOLOGY, minimum gate width: 2 ns).

Generating an arbitrary delay with a delay generator triggered by a Q-switch output signal of the laser, the ICCD camera was synchronized with single laser pulse and a discharge pulse, and then an image of the delay was captured at each pulse. Since the phenomena were highly reproducible, it was possible to obtain images of temporal behaviors of plasma formation and acceleration process with 2 ns resolution through changing the delay.

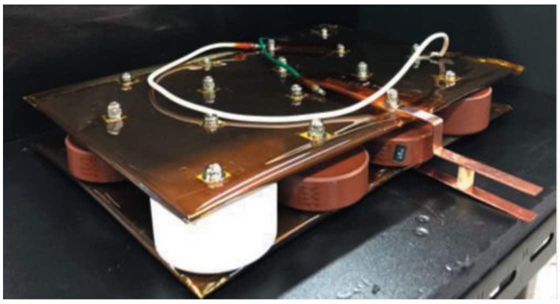

Figure 3. Laser Assisted Pulsed Plasma Thruster (LA-PPT).

Table 1. Configuration of LA-PPT

Channel length: ***l***	50 mm
Channel width: ***w***	10 mm
Channel gap: ***h***	15 mm
Electrode material	Mo
Propellant material	Al_2O_3

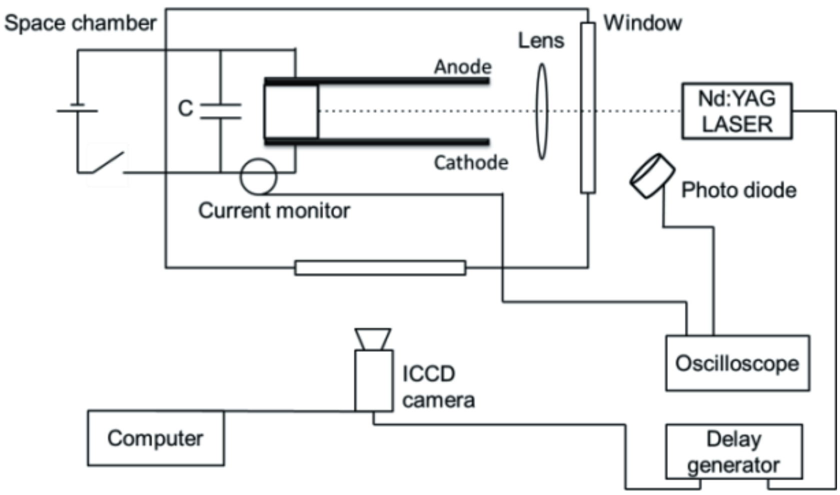

Figure 4. Schematic of experimental set up for ICCD camera observation.

B. Magnetic probe measurement

Temporal variations of magnetic field distributions in an acceleration channel, between anode and cathode, were estimated with magnetic probes. In this study, the magnetic probes were attached on a side wall (glass wall) of the acceleration channel, shown schematically in Fig.7, to insulate the coils from the electrodes. Each probe consists of a coil of a core diameter of 1 mm (3 turns of enameled copper wire of 0.6 mm in diameter). Positions of the magnetic probes on the glass wall, based on the rectangular coordinate system defined in Fig.6, are located at (x, y) = (0 mm, 7mm) for probe1, (x, y) = (0mm, 3.5mm) for probe2, (x, y) = (0 mm, 0mm) for probe3, (x, y) = (0 mm, -3.5mm) for probe4, and (x, y) = (0 mm, -7.5mm) for probe5, as shown in Fig.9. Moreover, each probe can be moved to the electrode edge horizontally by an x-axis stage.

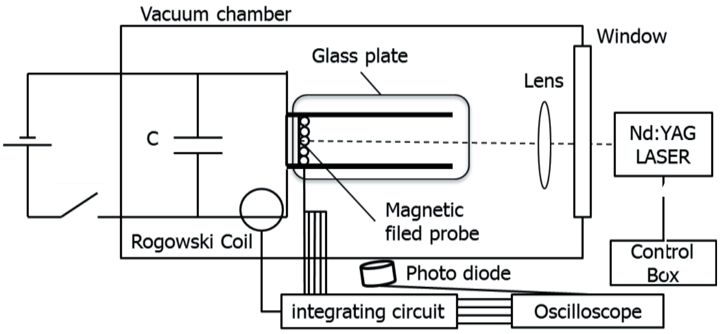

Figure 5. Schematic of experimental set up for magnetic field measurement.

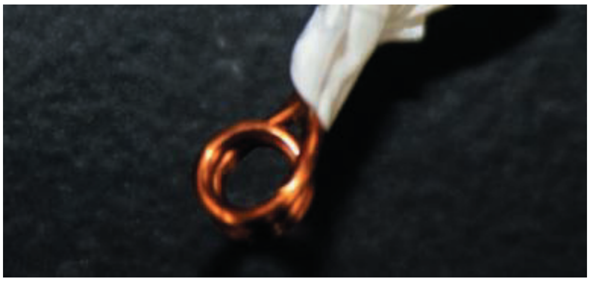

Figure 6. Magnetic field probe

Table 2 Configuration of Magnetic field probe

Turns	3
Coil radius	
Material	Enameled Copper Wire

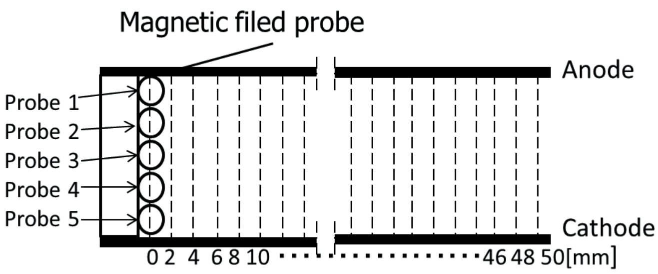

Figure 7. Positions of magnetic probes on side wall of acceleration channel.

V. Results and Discussion

A. Plasma behavior observation with ICCD camera

ICCD images of plasma plume from a short-pulse LA-PPT are shown in Fig. 10 for Vc = 10 kV, C=24nF respectively. In these figures, upper and lower white lines and a rectangular part corresponds to upper (anode) and lower (cathode) electrodes and a propellant surface, respectively. From this image, laser induced plasma can be seen at 0 ns. After 200 ns, a planar emission plasma can be observed on the propellant surface. Since this emission is running between the electrodes, this must be originated from the discharge. After 275 ns, strong emission spots can be seen at near electrodes (especially on lower electrode) and propellant surface. Although the maximum discharge current in this case was occurring at 500 ns, relatively stronger emissions can be seen at 400 ns. From these results, it was confirmed that no strong correlations between discharge current and plasma emissions can be extracted.

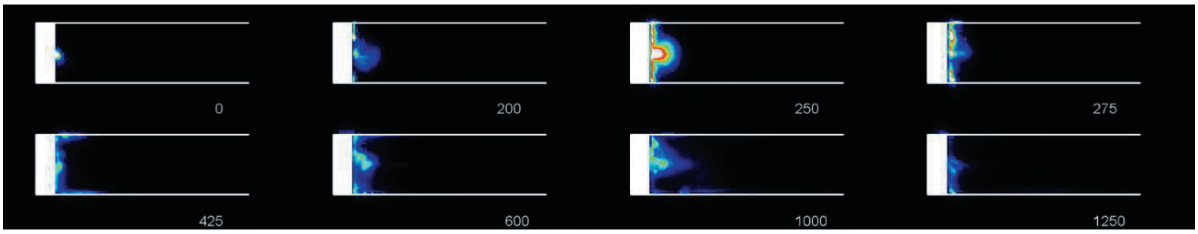

Figure 8. ICCD images of plume from a rectangular thruster (anode: higher electrode for td = 0-1250 ns, V_c = 10,000 V)

B. Magnetic field measurement

Temporal variations of magnetic fields measured by the magnetic probes located at various positions are shown in Figs.9, 10 (for V_c = 8,000 V, C = 24 nF), 11 and 12 (for V_c = 8,000 V, C = 50 nF). As can be seen, the magnetic fields in the acceleration channel were changing temporally and spatially. In general, it is presumed in PPT operation that the discharge current runs between electrodes forming a current sheet, and the motion of the current sheet is induced by an interaction of the discharge current in the current sheet and the self-induced magnetic field, or namely, Lorentz force. Associated with the motion of the current sheet, the motion of the magnetic fields in the acceleration channel will be induced. Since the magnetic probes are fixed on a side wall of the acceleration channel in this study, temporal variation of the magnetic field monitored with each probe includes positive and negative waveforms of the magnetic field. From Fig.12, it is shown that there are delays for the first positive (or negative) peaks at probes located at further downstream positions. These delays can be the durations for the magnetic field, or the current sheet, moving in the distances between the probes. Moreover, it can also be seen that temporal variations of the magnetic fields in regions at near propellant surface are almost in phase with a discharge current waveform. This implies that a portion of the discharge current is probably running at near surface of the propellant.

Temporal variations of magnetic fields measured by the magnetic probes located at various positions for V_c = 8,000 V, C = 24 nF are shown in Figs.9 (for $x = 0 \sim 50$ mm, Δx = 10 mm) and 10 (for $x = 0 \sim 10$ mm, Δx = 2 mm). Variations of magnetic field distributions regenerated from all the position of magnetic probes are shown in Fig.11. As can be seen in these figures, the magnetic fields in a whole region of the acceleration channel are induced at 250 ns after induction of discharge current between electrodes. Then, similar to the discharge current waveform, the magnetic field waveforms periodically change with average peak values of ±0.5 T.

From these results, it is shown that, in this case, magnetic field is induced in a whole region in the discharge channel and is oscillating with similar frequency to that of discharge current.

Temporal variations of magnetic fields measured by the magnetic probes located at various positions for V_c = 8,000 V, C = 50 nF are shown in Figs.12 (for $x = 0 \sim 50$ mm, Δx = 10 mm) and 13 (for $x = 0 \sim 10$ mm, Δx = 2 mm). Variations of magnetic field distributions regenerated from all the position of magnetic probes are shown in Fig.14. From these figures, the magnetic field at x = 0 mm is induced at 250 ns after induction of discharge current and the magnetic field reaches up to 0.12 T. At 10 ~ 50 mm, generation of the magnetic field can also be confirmed.

In a near surface region of the propellant shown in Figs.12 and 13, the maximum magnetic field is observed at x = 0 mm at 250 ns. At $x = 2 \sim 10$ mm, the maximum magnetic fields are observed where each signal is following a former signal with an almost constant delay. These delays can be the durations for the magnetic field, or the current sheet, to move in the distances between the probes.

From these figures, the strength of magnetic field is decreasing with increasing distance from the propellant surface, or approaching the electrode edge. In particular, this tendency becomes more drastic especially at positions of x> 10 mm. From these results, it is confirmed that magnetic field strength in near surface region of $x = 0 \sim 10$ mm is much stronger than those measured in the other regions.

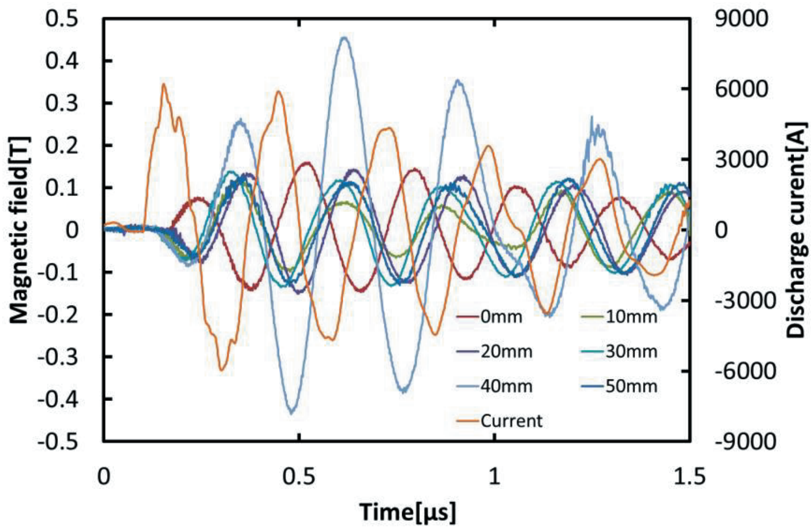

Figure9. Probe 3 signal at 0~50 mm from propellant surface (Vc =8,000V,C=24nF)

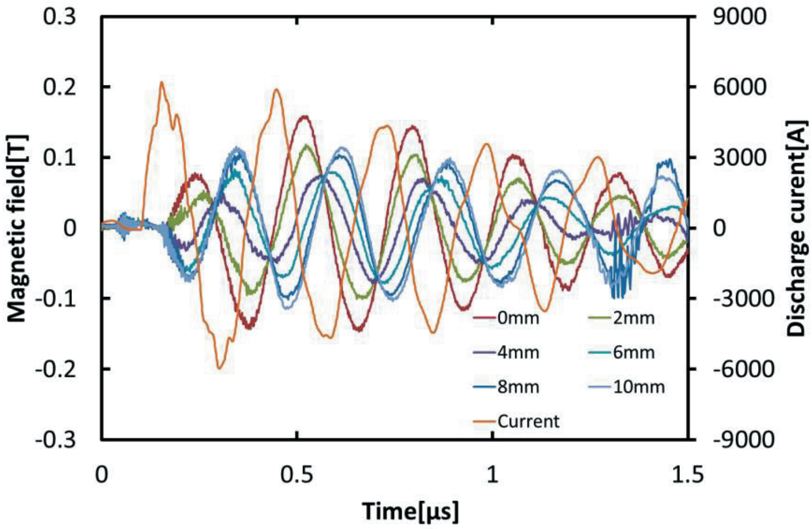

Figure10. Probe 3 signal at 0~10 mm from propellant surface (Vc =8,000V,C=24nF)

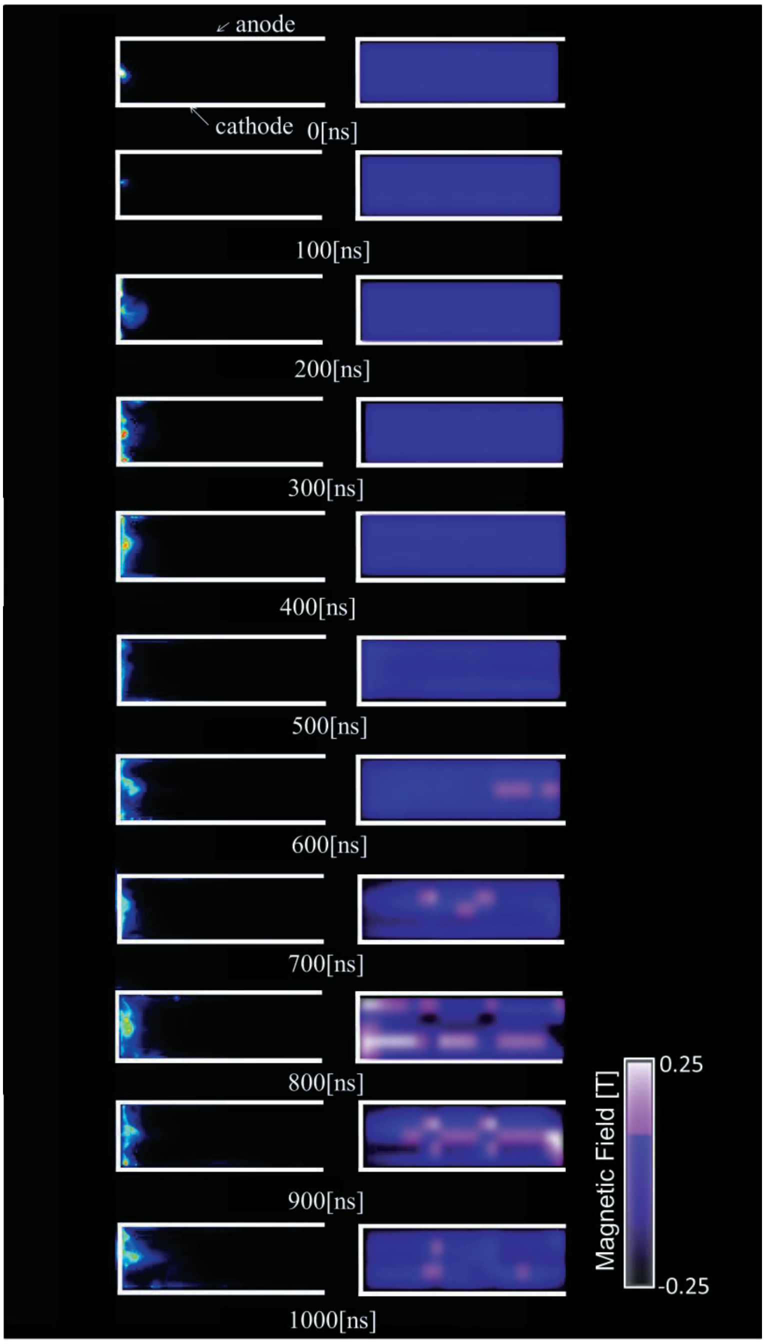

Figure.11 Temporal variation of magnetic field distribution (right) (for td = 0 ~ 1000 ns, Vc =8,000 V) and ICCD camera images (left) in acceleration channel (for td = 0 ~ 1000 ns, Vc =10,000 V)

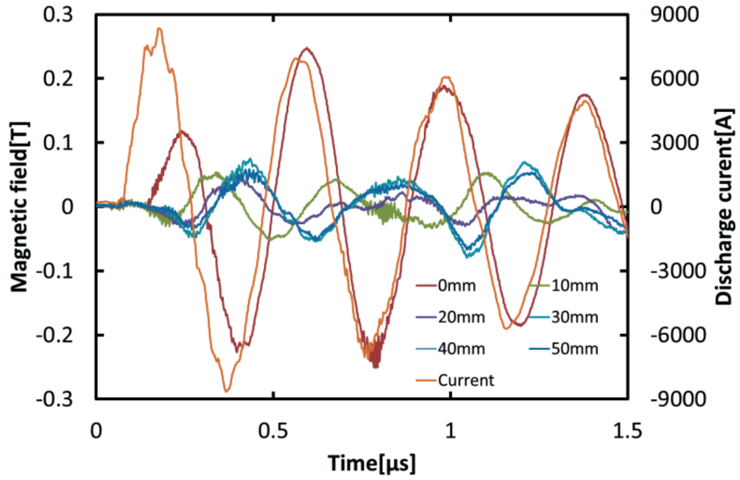

Figure12. Probe 3 signal at 0~50 mm from propellant surface (Vc =8,000V,C=50nF)

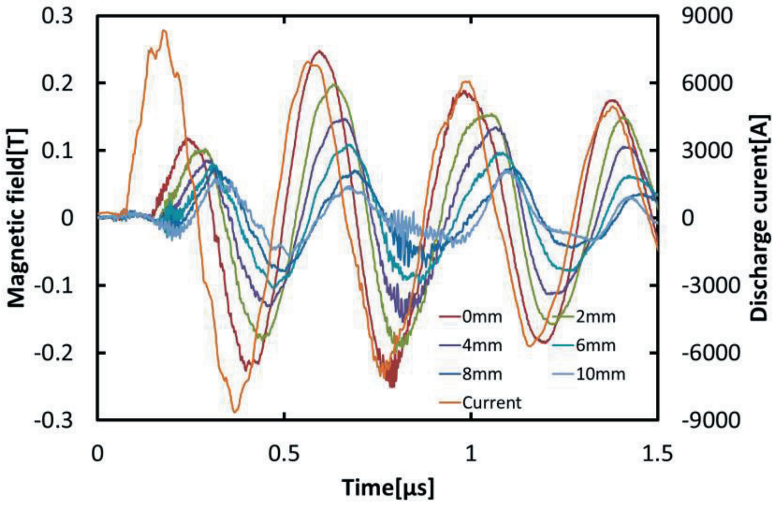

Figure13. Probe 3 signal at 0~10 mm from propellant surface (Vc =8,000V,C=50nF)

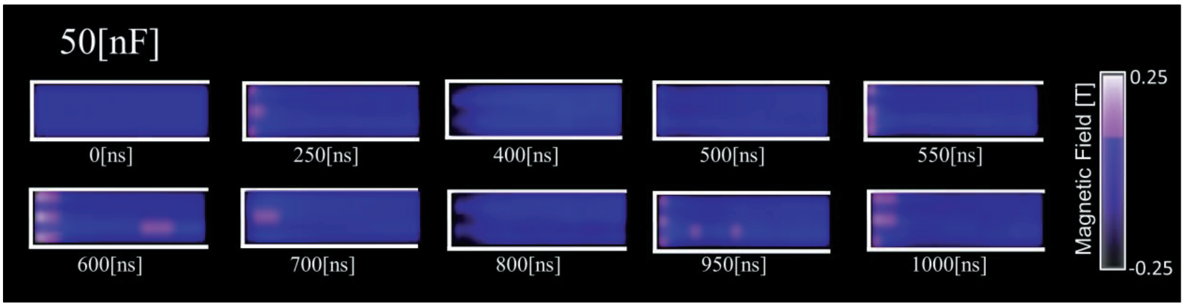

Figure.14 Temporal variation of magnetic field distribution (left) (for *t*d = 0 ~ 1000 ns, *V*c =8,000 V, *C*=24nF) and (right) (for *t*d = 0 ~ 1000 ns, *V*c =8,000 V, *C*=50nF) in acceleration channel

VI. Conclusion

To observe the plasma acceleration process and to understand the mechanism of high speed plasma generation between the rectangular electrodes of a short-pulse laser-assisted pulsed plasma thruster (LA-PPT), observation of plasma behaviors by an ICCD camera and measurement of magnetic field distributions by magnetic probes were conducted. From the time-resolved ICCD images, behaviors of the plasma wavefront were analyzed. From the results of time-resolved images, the strong emission regions were found at near electrodes and propellant surface. Furthermore, it was confirmed that no strong correlations between discharge current and plasma emissions could be extracted.

In addition, temporal variations of magnetic field distributions were measured by magnetic field probes located at various positions for V_c = 8,000 V (C = 24, 50 nF). From the result, magnetic field was induced in a whole region in the discharge channel and was oscillating with similar frequency to that of discharge current for C = 24 nF. On the other hand, for the C = 50 nF, the strength of magnetic field was decreasing with increasing distance from the propellant surface. It was confirmed that magnetic field strength in near surface region of $x = 0 \sim 10$ mm was much stronger than those measured in the other regions.

References

1) Myers, R. M., et al.: Small Satellite Propulsion Options, AIAA Paper, 1994, pp. 94-2997.

2) Mueller, J.: Thruster Options for Microspacecraft: A Review and Evaluation of Existing Hardware and Emerging Technologies, AIAA Paper, 1997, 97-3058,.

3) Leifer, S.: Overview of NASA's Advanced Propulsion Concepts Activities, AIAA Paper, 1998, 98-3183.

4) Micci, M. M., and Ketsdever, A. D. (ed.): Micropropulsion for Small Spacecraft, American Institute of Aeronautics and Astronautics, *Astronautics and Aeronautics.,* **187** (2000).

5) Gonzales, D., and Baker, R.: Micropropulsion Using a Nd:YAG Microchip Laser, Proceedings of SPIE

6) Pakhomov, A.V., et al.: Specific Impulse Study of Ablative Laser Propulsion, AIAA Paper, 2001, 2001-3663.

7) Horisawa, H., and Kimura I.: Fundamental Study on Laser Plasma Accelerator for Propulsion Applications, *Vacuum*, **65** (2002), pp.389-396.

8) Horisawa, H., et al., Beamed Energy Propulsion: AIP Conference Proceedings, **664** (2003), pp.423-432.

9) Kawakami, M., et al., AIAA Paper, 2003, 2003-5028.

10) Horisawa, H., et al., *Applied Physics A*., **81** (2005), pp.303-310.

11) Horisawa, H., et al., The Review of Laser Engineering., **34** (2006), pp.435-441.

12) Sasaki, Y., et al., IEPC (International Electric Propulsion Conference) Paper, 2007-56.

13) Horisawa, H., et al, AIAA Paper, 2008, 2008-4818.

14) Ono, T., et al, AIAA Paper, 2008, 2008-5008.

15) Horisawa, H.: High Isp Mechanism of Rectangular Laser-Electromagnetic Hybrid Acceleration Thruster, IEPC (International Electric Propulsion Conference) Paper IEPC-2011-274, pp. 7-8

16) T.E. Markusic.: Phenomenological Model of Current Sheet Canting in Pulsed Electromagnetic Accelerators, IEPC (International Electric Propulsion Conference) Paper, 2003, 2003-0293, pp. 5-6

17) Jahn, R. G.: *Physics of Electric Propulsion*, McGraw-Hill, 1968, pp.198-316.

18) Burton, R. L., and Turchi, P. J.: Pulsed Plasma Thruster, *Journal of Propulsion and Power.,* **14** (1998), pp. 716–735.

19) A. Nawaz, M. Lau, G. Herdrich, and M. Auweter-Kurtz. "Investigation of the Magnetic Field in a Pulsed Plasma Thruster", AIAA Journal, Vol. 46, No. 11 (2008), pp. 2881-2889.

20) T.E. Markusic, E.Y. Choueiri. "Photographic, magnetic, and interferometric measurements of current sheet canting in a pulsed electromagnetic accelerator" AIAA Paper, 2001 ,2001-3896